

Communication-Efficient Hybrid Language Model via Uncertainty-Aware Opportunistic and Compressed Transmission

Seungeun Oh, Jinhyuk Kim, Jihong Park, Seung-Woo Ko, Jinho Choi, Tony Q. S. Quek, and Seong-Lyun Kim

Abstract—To support emerging language-based applications using dispersed and heterogeneous computing resources, the hybrid language model (HLM) offers a promising architecture, where an on-device small language model (SLM) generates draft tokens that are validated and corrected by a remote large language model (LLM). However, the original HLM suffers from substantial communication overhead, as the LLM requires the SLM to upload the full vocabulary distribution for each token. Moreover, both communication and computation resources are wasted when the LLM validates tokens that are highly likely to be accepted. To overcome these limitations, we propose *communication-efficient and uncertainty-aware HLM (CU-HLM)*. In CU-HLM, the SLM transmits truncated vocabulary distributions only when its output uncertainty is high. We validate the feasibility of this opportunistic transmission by discovering a strong correlation between SLM’s uncertainty and LLM’s rejection probability. Furthermore, we theoretically derive optimal uncertainty thresholds and optimal vocabulary truncation strategies. Simulation results show that, compared to standard HLM, CU-HLM achieves up to $206\times$ higher token throughput by skipping 74.8% transmissions with 97.4% vocabulary compression, while maintaining 97.4% accuracy.

Index Terms—Large language model (LLM), speculative decoding, uncertainty, opportunistic transmission, on-device LLM.

I. INTRODUCTION

LARGE language models (LLMs), with their massive parameter counts and rich training data, have demonstrated remarkable emergent capabilities [1]. These capabilities span a wide range of applications, including open-domain question answering, code generation, commonsense reasoning, and even robotic control [2]–[6]. To seamlessly adopt LLMs into a wireless edge environment, the hybrid language model (HLM) framework [7] has emerged, which physically splits the inference task between an on-device small language model (SLM) and a remote LLM. Specifically, given a token—a basic unit of text generation such as a word or subword fragment—and the corresponding vocabulary, which denotes the full set of possible tokens the model can output, the SLM proposes a draft token based on a given prompt, which is then transmitted to the server. The server-side LLM then decides whether to accept or resample it. This speculative decoding approach [8] ensures that the output distribution matches that

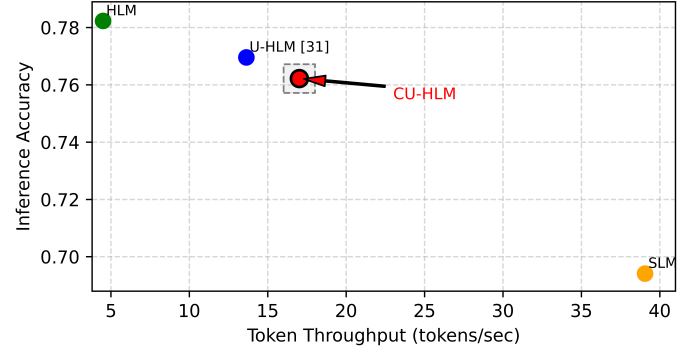


Fig. 1: Comparison of inference accuracy and token throughput, where token throughput is inversely proportional to end-to-end latency, including communication and computation delays (SNR 10 dB, Rayleigh fading).

of the LLM, preserving inference accuracy while relieving the LLM’s computation burden.

Despite these advantages, HLM suffers from severely limited token throughput due to its architectural overhead. According to our simulations, to be detailed in Section V, each token generation requires: (i) SLM-to-LLM uplink transmission of the full 32,000-token vocabulary distribution, incurring up to 92 kB of payload per token; and (ii) execution of both SLM and LLM inference, which take 25.6 ms and 104.6 ms, respectively—limiting the overall token throughput to fewer than 5 tokens per second under 10 MHz uplink bandwidth.

To address the token throughput bottleneck inherent in HLMs, in this paper, we propose communication-efficient and uncertainty-aware HLM (**CU-HLM**) that reduces uplink communication and server-side computation overhead. CU-HLM introduces two key innovations: *uncertainty-aware opportunistic transmission*, which skips both uplink transmission and remote LLM computation when the SLM’s uncertainty is below a threshold; and *uncertainty-aware compressed vocabulary transmission*, which transmits only the top- k token probabilities, with k increasing with the SLM’s uncertainty. These methods were motivated by our experimental findings: a strong linear correlation between the SLM’s uncertainty and the LLM’s rejection probability; and the optimal k increasing with the token’s uncertainty. Leveraging these uncertainty-aware methods with our theoretically derived optimal k and uncertainty threshold, CU-HLM achieves an effective trade-off between token throughput and inference accuracy, as illustrated in Figure 1.

S. Oh, J. Kim, and S.-L. Kim are with the School of Electrical and Electronic Engineering, Yonsei University, Korea.

J. Park and T. Q. S. Quek are with the Information Systems Technology and Design pillar, Singapore University of Technology and Design, Singapore.

S.-W. Ko is with the Department of Smart Mobility Engineering, Inha University, Korea.

J. Choi is with the School of Electrical and Mechanical Engineering, The University of Adelaide, Australia.

A. Related Works

LLMs such as Meta’s Llama series [9], Google’s Gemma [10], and DeepSeek [11] have demonstrated strong performance across a variety of tasks, including reasoning, information retrieval, and dialogue generation [6]. However, their high computational complexity and memory demands make them impractical for on-device deployment [12], [13]. As a result, LLMs are typically hosted on remote servers, leading to considerable inference latency over wireless networks. This limitation has motivated the development of SLMs, such as TinyLlama [14], Phi-2 [15], and MobileVLM [16], as well as quantized LLMs [17], which enable lightweight inference that can be executed directly on mobile devices. To further enhance the effectiveness of these models, numerous techniques such as model pruning, quantization, and knowledge distillation have been explored [18]–[20]. Nevertheless, these approaches often come at the cost of reduced inference accuracy [21], [22], underscoring the trade-off between latency and accuracy in mobile AI deployment.

To address the latency-accuracy trade-off in wireless edge inference, HLMs have been considered an attractive solution by leveraging both device-side and server-side computing resources [7], [17], [23], [24]. In the HLM framework, a SLM is deployed on the device, and a LLM resides on the network edge server. Inspired by speculative inference [8], [25], the HLM operates in two stages: the on-device SLM first generates a draft token in response to the user query, and the server-side LLM subsequently verifies whether the token should be accepted or resampled. This collaborative inference process ensures that the resulting output distribution is consistent with that of the LLM alone, thereby preserving accuracy while distributing the computational load.

However, the HLM architecture causes additional communication and computation overheads. Specifically, for each token, the SLM must transmit its full vocabulary distribution to the server to enable verification or correction. In addition, both the SLM and LLM must perform inference for every token generation. This communication and dual computation requirement brings about considerable latency, limiting token throughput. The conventional approaches focusing on computation aspects, such as quantization, model compression, and optimized CPU/GPU memory allocation [17], [26]–[28], can be ineffective since the issue of communication burden is ignored. To address this, early studies such as [29] propose query-level offloading to address the issue, where the entire input is directed either to the on-device SLM or to the server-side LLM based on the estimated difficulty of the query. While simple and effective at a coarse level, such approaches lack the granularity needed for token-level control.

Recent research moves towards joint optimization of communication and computation by selectively determining which tokens should be sent to the LLM for verification. For instance, [7] computes the acceptance probability of each token using the LLM, but this approach still requires full LLM computation for every token. Other works leverage auxiliary AI techniques—such as multi-layer perceptrons (MLPs) [23] or reinforcement learning [30]—to determine whether

individual tokens should be forwarded to the server. While these methods offer flexible token-level control, they incur additional training computation and require architectural modifications, potentially limiting their feasibility in real-time or resource-constrained edge deployments. Building upon these prior works, we aim to improve HLM throughput by jointly optimize communication and computation, while maintaining inference accuracy.

B. Contributions and Paper Organization

The main contributions of this paper are outlined below:

- We propose **CU-HLM**, which applies opportunistic and compressed vocabulary transmission based on the SLM’s uncertainty. The rationale behind this design is supported by empirically discovering strong correlations among the SLM’s uncertainty, the LLM’s rejection probability, and the vocabulary compression size.
- For uncertainty-aware opportunistic transmission, we theoretically derive the maximum uncertainty threshold that guarantees the unbiasedness condition, i.e., ensuring that HLM’s output distribution aligns with that of the LLM. For uncertainty-aware vocabulary compression, we derive a theoretical upper bound on the resulting bias, thereby determining the minimum vocabulary truncation size.
- To apply these optimal uncertainty threshold and vocabulary compression, the SLM requires access to the LLM’s outputs. Assuming known LLM output statistics, we propose **CU-HLM (Offline)**, where the vocabulary compression size is fixed based on an average bias constraint. By relaxing the bias upper bound to remove LLM dependency, we further develop **CU-HLM (Online)**, which dynamically adjusts the vocabulary size according to each token-level bias constraint.
- Extensive simulations across wireless fading channels, SNRs, datasets, and model configurations show that CU-HLM (Online) achieves **97.4%** of HLM accuracy and up to **206×** higher token throughput under poor wireless channel conditions, while reducing uplink transmissions by **74.8%** (85.7% of them are finally accepted) and transmitting only **2.6%** of the full vocabulary payload.

Note that the conference version [31] of this work presents only the uncertainty-aware opportunistic transmission, termed U-HLM. To further improve communication efficiency and token throughput, this work additionally introduces uncertainty-aware vocabulary compression, which poses new challenges in optimizing vocabulary compression size and designing online/offline strategies. By theoretically deriving the optimal settings, the proposed CU-HLM (Online) achieves 17.6% higher token throughput and a 177.5× communication latency reduction, compared to U-HLM in [31].

The remainder of this paper is organized as follows: Section II presents a systematic overview of the HLM framework, including its integration with wireless communication systems and the definition of token throughput. Section III explores the relationship between token-level uncertainty and LLM rejection probability, and introduces U-HLM by extending the

HLM framework with uncertainty-aware opportunistic transmission along with a theoretically derived optimal uncertainty threshold. Section IV then proposes CU-HLM by integrating a vocabulary compression scheme with U-HLM, and describes its offline and online variants based on optimal vocabulary size selection. Section V provides a comprehensive empirical evaluation, examining the effects of uncertainty thresholds and vocabulary sizes, validating CU-HLM across various settings, and including an ablation study on the impact of SLM architecture and alignment on token throughput. Finally, Section VI concludes the paper.

II. SYSTEM MODEL

The network considered in this study comprises a single device and a base station (BS) equipped with a powerful server. In accordance with the HLM architecture proposed in [7], the device and server are respectively equipped with a SLM and a LLM. Both the SLM and LLM operate on basic units called tokens and share a common vocabulary \mathcal{V} , which defines the complete set of possible tokens. The task is to generate response tokens, given an input token sequence denoted by \mathbf{s} , by sampling from the model's vocabulary distribution.

A. Token Generation of a Hybrid Language Model

The core inference mechanism in the HLM consists of two stages: (1) draft token generation by the SLM, and (2) verification and potential correction by the LLM through resampling. Further details are provided below.

Step 1: SLM's Draft Generation. In the t -th round, the input to the SLM, denoted by $\mathbf{s}(t)$, is constructed by concatenating the input token sequence \mathbf{s} with the cumulative response token sequence up to the $(t-1)$ -th round, denoted by $\mathbf{r}(t-1)$: $\mathbf{s}(t) := \mathbf{s} \oplus \mathbf{r}(t-1)$, where \oplus denotes the concatenation operator.

The SLM processes $\mathbf{s}(t)$ and generates a logit vector $\mathbf{z}(t) = [z_1(t), z_2(t), \dots, z_{|\mathcal{V}|}(t)]^\top$. This logit vector is then normalized to obtain the SLM's vocabulary distribution $\mathbf{x}(t) = [x_1(t), x_2(t), \dots, x_{|\mathcal{V}|}(t)]^\top$, where:

$$x_v(t) = \frac{\exp(z_v(t))}{\sum_{i=1}^{|\mathcal{V}|} \exp(z_i(t))}, \quad \forall v \in \mathcal{V}. \quad (1)$$

The SLM then samples a draft token d from this distribution, i.e., $d \sim \mathbf{x}(t)$.

Step 2: LLM's Verification & Correction. The LLM also processes $\mathbf{s}(t)$ to produce a logit vector, which is then normalized to yield its own vocabulary distribution: $\mathbf{y}(t) = [y_1(t), y_2(t), \dots, y_{|\mathcal{V}|}(t)]^\top$. It then compares the probabilities assigned to the draft token $d \in \mathcal{V}$ under both the SLM and LLM distributions. The verification and refinement proceeds as follows:

- **Case 1 (Deterministic Acceptance):** If $y_d(t) \geq x_d(t)$, the draft token is accepted by the LLM.
- **Case 2-1 (Probabilistic Acceptance):** If $y_d(t) < x_d(t)$, the draft token is accepted with probability $y_d(t)/x_d(t)$.
- **Case 2-2 (Reject & Resampling):** If $y_d(t) < x_d(t)$ and the draft token is rejected (with probability $1 -$

$y_d(t)/x_d(t)$), the target token d^* is sampled from the resampling distribution $\mathbf{p}(t) = [p_1(t), p_2(t), \dots, p_{|\mathcal{V}|}(t)]^\top$, i.e., $d^* \sim \mathbf{p}(t)$, where:

$$p_v(t) = \frac{(y_v(t) - x_v(t))^+}{\sum_{i=1}^{|\mathcal{V}|} (y_i(t) - x_i(t))^+}, \quad \forall v \in \mathcal{V}, \quad (2)$$

in which $(\cdot)^+ = \max(0, \cdot)$ is the ReLU function.

The final response token $r(t)$ is set to d in **Case 1** and **Case 2-1**, where the draft token is accepted, and to d^* in **Case 2-2**, where resampling occurs. This completes one round of token generation in the HLM framework.

This mechanism is inspired by speculative decoding methods [8], [25], and is carefully constructed to satisfy an *unbiasedness condition*, ensuring that the overall output distribution of HLM inference matches that of the original LLM:

$$x_v(t) \cdot (1 - \beta_v(t)) + \left(\sum_i (x_i(t) \cdot \beta_i(t)) \right) \cdot p_v(t) = y_v(t), \quad \forall v, \quad (3)$$

where $\beta_v(t) = \left(1 - \frac{y_v(t)}{x_v(t)}\right)^+$ denotes the rejection probability of the v -th token.

Each term in (3) has a clear interpretation, directly corresponding to the three possible cases in the LLM verification process. The first term, $x_v(t) \cdot (1 - \beta_v(t))$, represents the probability that token v is accepted as the response token—either deterministically as in **Case 1** or probabilistically as in **Case 2-1**. The second term, $(\sum_i (x_i(t) \cdot \beta_i(t))) \cdot p_v(t)$, accounts for the overall probability that token v is selected through resampling in **Case 2-2**, averaged over all possible draft tokens that may be rejected. The right-hand side (RHS), $y_v(t)$, denotes the target probability assigned to token v by the full LLM inference. This equality serves as a core theoretical condition that ensures the inference accuracy of the HLM framework. Moreover, this condition underpins the design of uncertainty-aware skipping and vocabulary compression, which will be elaborated in later sections.

To proceed to the next round, the response sequence is updated in an autoregressive manner: $\mathbf{r}(t) = \mathbf{r}(t-1) \oplus r(t)$, so that the newly generated token becomes part of the input for the next step. This iterative procedure continues until the sequence reaches its maximum length $|\mathbf{r}(t)| = r_{\max}$ or an End-of-Sentence (EOS) token is generated.

B. Wireless Communication

The HLM inference process requires both uplink and downlink transmissions between the device and the BS. For the uplink, after the SLM generates a draft token, the device transmits: 1) the index of the draft token d within the vocabulary, and 2) a set of indices and corresponding probabilities from the vocabulary distribution $\mathbf{x}(t)$ of (1), enabling the LLM to perform verification and, if necessary, resampling. Subsequently, the device downloads the index of the final response token—either the accepted draft token d or a resampled target token d^* .

For simplicity, we assume that the communication cost incurred by transmitting token indices is negligible. This

allows us to account only for the uplink transmission of the vocabulary distribution, whose payload size B is given by:

$$B = |\mathcal{V}|(b_{\text{prob}} + b_{\text{index}}) \text{ (in bits)}, \quad (4)$$

where b_{prob} and b_{index} denote the number of bits required to represent a probability value and a vocabulary index, respectively. For indices, binary encoding is assumed, yielding $b_{\text{index}} = \lceil \log_2 |\mathcal{V}| \rceil$.

We adopt a block fading model for the wireless channel, where the channel gain remains constant within each round but may vary from one round to another. The uplink transmission time for the t -th round, denoted by $\tau(t)$, is calculated using Shannon's capacity formula as:

$$\tau(t) = \frac{B}{W \log_2(1 + \text{SNR}(t))} \text{ (in sec)}, \quad (5)$$

where W represents the bandwidth of the uplink channel. The signal-to-noise ratio (SNR) at the t -th round, expressed as $\text{SNR}(t)$, depends on the transmit power p of the device, the distance ρ to the BS, the path loss exponent α , and the noise power N .

C. Token Throughput

To quantify the token generation rate of the HLM while accounting for both communication and computation latency, we introduce the notion of *token throughput*, defined as the number of response tokens generated per unit time. For tractability, we assume that the SLM and LLM incur constant per-token computation times, denoted by τ_{SLM} and τ_{LLM} , respectively. Then, the token throughput at the t -th round, denoted by $\text{TP}(t)$, is given by:

$$\text{TP}(t) = \frac{1}{\tau_{\text{SLM}} + \tau(t) + \tau_{\text{LLM}}} \text{ (tokens/sec)}. \quad (6)$$

Despite its architectural advantages, HLM inference suffers from a fundamental limitation—its low token throughput, as quantified in (6). Each token generation involves not only computation on both the SLM and LLM but also significant communication overhead, including the transmission of a payload proportional to the full vocabulary distribution size as defined in (4). According to (6), increasing token throughput requires reducing the overall latency, particularly the LLM computation latency τ_{LLM} and the uplink communication latency $\tau(t)$. The following schemes address this by improving transmit opportunity and reducing uplink communication cost, respectively.

III. UNCERTAINTY-AWARE OPPORTUNISTIC HYBRID LANGUAGE MODEL

In this section, we introduce the *Uncertainty-Aware Opportunistic HLM (U-HLM)*. This approach enables the device to opportunistically skip both uplink transmission and LLM computation when the uncertainty—quantified via temperature perturbation [32]—falls below a predefined threshold. We begin by examining whether the rejection probability of a draft token can be predicted solely from on-device uncertainty estimates. We then derive an optimal threshold that balances token throughput and inference accuracy. The SLM, LLM, and datasets used are consistent with those described in Section V.

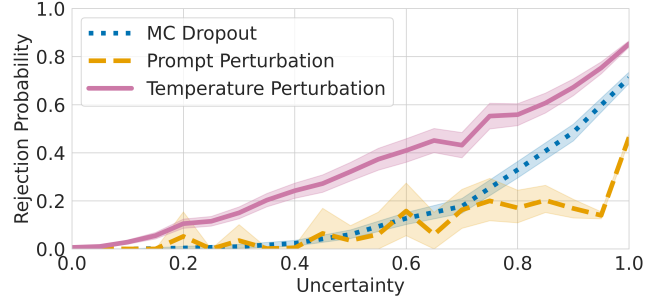


Fig. 2: Uncertainty vs. rejection probability. Solid lines show mean; shaded regions denote 95% CI. Correlation coefficients: temperature perturbation (0.71), MC Dropout (0.65), and prompt perturbation (0.20).

A. Uncertainty and Rejection Prediction

Inspired by the concept of uncertainty—quantifying how confident a model is in its output—we explore its applicability within the HLM framework. Specifically, we hypothesize that the SLM can predict the LLM's rejection probability $\beta_d(t)$ for a draft token d based on its own uncertainty estimate during token generation.

To validate this hypothesis, we conduct experiments using representative uncertainty estimation techniques, including (1) sample-based methods [33] (Bayesian methods such as MC Dropout [34]) and (2) perturbation-based methods [32] (test-time augmentation methods such as prompt perturbation and temperature perturbation). In the MC Dropout setting, we apply dropout to the SLM using 20 dropout probabilities sampled uniformly from the range $[0, 0.1]$, sampling one token per dropout configuration. For prompt perturbation, we generate 20 paraphrased versions of the input token sequence using WordNet [35] and sample a token for each paraphrased prompt. For temperature perturbation, we sample 20 temperatures uniformly from $[0, \theta_{\text{max}} = 2]$, and generate a token per temperature setting. The uncertainty for each method is then computed as the average distance between the generated tokens and the draft token, aiming to quantify the dispersion of the sampled outputs; further details on the uncertainty computation will be introduced later.

Figure 2 shows the correlation between the uncertainty and rejection probability across these methods, leading to the following observations:

- All three uncertainty measures exhibit a positive correlation with the rejection probability.
- Temperature perturbation demonstrates the clearest linear trend across a wide range of uncertainty values and yields the highest correlation coefficient (0.7106).

These results suggest that temperature perturbation is the most effective approach for predicting rejection probability among the techniques we concern. Accordingly, we formalize this insight:

Remark 1 (Linear Correlation Between Uncertainty and Rejection Probability). *For every t -th round in HLM inference, the uncertainty $u(t)$ measured via temperature perturbation*

exhibits a linear relationship with the LLM's rejection probability $\beta_d(t)$ for the SLM-generated draft token d as:

$$\beta_d(t) = a \cdot u(t) + b, \quad \forall t, \quad (7)$$

where $a = 0.815$ and $b = -0.066$ are obtained through linear regression, with a mean squared error (MSE) of 1.41×10^{-3} and a coefficient of determination of 0.9774.

B. Uncertainty-Aware Opportunistic Transmission.

Motivated by **Remark 1**, we propose U-HLM as described below. The proposed framework operates on top of the standard HLM token generation pipeline, preserving **Step 1** (draft generation) and **Step 2** (LLM verification), while introducing an additional mechanism between them. This intermediate process is illustrated in Figure 3. To facilitate explanation, we define a binary indicator variable $\delta(t) \in \{0, 1\}$, where $\delta(t) = 1$ indicates that uplink transmission and LLM computation are performed in the t -th round, and $\delta(t) = 0$ otherwise.

In the t -th round, the device estimates uncertainty using temperature perturbation. Specifically, it samples M temperature values from the interval $[0, \theta_{\max}]$, denoted $\{\theta^{(1)}, \dots, \theta^{(M)}\}$. For each sampled temperature $\theta^{(m)}$, the device applies it to the SLM's softmax operation (as defined in (1)) to produce a perturbed vocabulary distribution $\tilde{\mathbf{x}}^{(m)}(t)$, whose v -th element is defined as:

$$\tilde{x}_v^{(m)}(t) = \frac{\exp(z_v(t)/\theta^{(m)})}{\sum_{i=1}^{|\mathcal{V}|} \exp(z_i(t)/\theta^{(m)})}, \quad \forall v \in \mathcal{V}. \quad (8)$$

From each $\tilde{\mathbf{x}}^{(m)}(t)$, a token $d^{(m)}$ is sampled, and the uncertainty $u(t)$ is computed as the average disagreement between these samples and the original draft token d :

$$u(t) = \frac{1}{M} \sum_{m=1}^M \mathbb{1}(d^{(m)} \neq d), \quad (9)$$

where $\mathbb{1}(\cdot)$ is the indicator function¹. Based on this uncertainty, the model opportunistically decides to skip uplink transmission according to:

$$\delta(t) = \begin{cases} 0, & \text{if } u(t) \leq u_{\text{th}}, \\ 1, & \text{otherwise.} \end{cases} \quad (10)$$

Skipping uplink transmission ($\delta(t) = 0$) may lead to a misalignment between the token sequences on the device and server sides. To avoid it, resynchronization requires additional index exchanges between the device and the BS, although the communication cost of these indices is considered negligible in this study.

C. Uncertainty Threshold

This subsection focuses on designing the uncertainty threshold to maximize communication efficiency while ensuring that the inference degradation remains bounded. In the context of U-HLM, inference degradation occurs when a draft token

¹Regarding the concern that uncertainty estimation may increase the SLM's computation overhead, we note that it is fully parallelized with the standard forward pass and thus does not introduce additional latency.

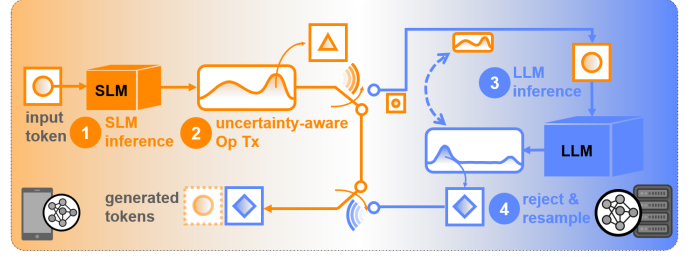


Fig. 3: Schematic illustration of U-HLM framework.

that would have been rejected by the LLM is mistakenly skipped—i.e., a false positive. We define the probability of such events as the U-HLM's rejection risk R , which exhibits a fundamental trade-off with communication efficiency, governed by the choice of uncertainty threshold. Accordingly, our goal is to determine an uncertainty threshold to minimize communication cost without allowing the rejection risk R to exceed a tolerable bound.

Recall that in the HLM framework, a draft token d is rejected when $y_d(t) < x_d(t)$, with a rejection probability given by $1 - y_d(t)/x_d(t)$. From the device's perspective, $x_d(t)$ is fixed once d is selected, while $y_d(t)$ remains a latent and inaccessible random variable. Consequently, the expected rejection probability $\mathbb{E}[\beta_d(t)]$ conditioned on a fixed draft token probability $x_d(t)$ can be expressed as:

$$\mathbb{E}_{y_d(t)}[\beta_d(t)] = P(y_d(t) < x_d(t)) \mathbb{E}_{y_d(t)} \left[1 - \frac{y_d(t)}{x_d(t)} \mid y_d(t) < x_d(t) \right]. \quad (11)$$

Given that the correlation between uncertainty and rejection probability exhibits only minor deviations (see Figure 2), we approximate $\mathbb{E}[\beta_d(t)] \approx \beta_d(t)$, which is now able to leverage the linear relationship in (7).

For analytical tractability, we assume that the uncertainty $u(t)$ and the rejection probability $\beta_d(t)$ are independent and identically distributed (i.i.d.) over time. Under this assumption, a fixed uncertainty threshold can be derived uniformly across rounds, as formalized in the following result:

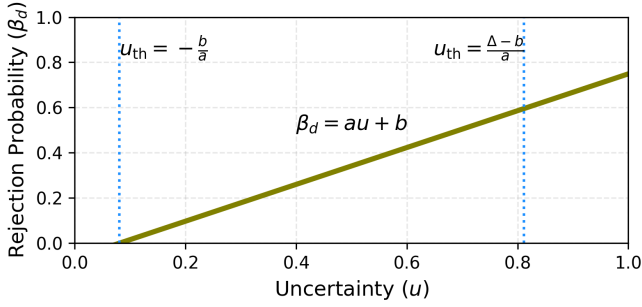
Theorem 1 (Uncertainty Threshold and Rejection Risk). *Assuming i.i.d. uncertainty $u(t)$ and rejection probability $\beta_d(t)$, let $u := u(t)$ and $\beta := \beta_d(t)$ for any t . Besides, we regard β equivalent to its expectation $\mathbb{E}[\beta]$ of (11). Then, the uncertainty threshold u_{th} is given as the upper limit:*

$$u_{\text{th}} = \frac{\Delta - b}{a}, \quad (12)$$

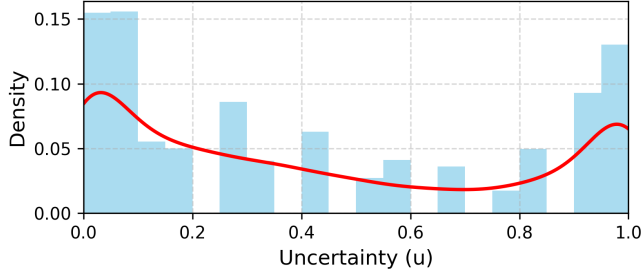
where $\Delta = P(y_d < x_d)$ denotes the probability that a token is not deterministically accepted. The resultant rejection risk R when skipping tokens with $u \leq u_{\text{th}}$ is upper bounded as

$$R \leq \frac{\Delta^{3/2}}{\sqrt{3a}} \cdot \sqrt{\int_{u=-\frac{b}{a}}^{\frac{\Delta-b}{a}} |f(u)|^2 du}, \quad (13)$$

where $f(u)$ denotes the probability density function (PDF) of the uncertainty u .



(a) Linear relationship between uncertainty and rejection probability. Dashed vertical lines indicate the theoretical risk-averse and risk-prone thresholds, respectively.



(b) Probability Density Function (PDF) of uncertainty, obtained via Gaussian kernel density estimation (KDE).

Fig. 4: Empirical characterization of two uncertainty thresholds and the density of the uncertainty values.

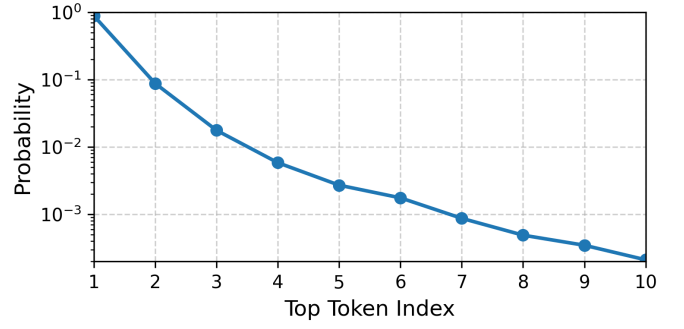
Proof. Since $0 < \mathbb{E}_{y_d} \left[1 - \frac{y_d}{x_d} \mid y_d < x_d \right] \leq 1$, it follows from (11) that $0 < \beta \leq \Delta$. Using the linear relationship in (7), the uncertainty range can be bounded as:

$$-\frac{b}{a} < u \leq \underbrace{\frac{\Delta - b}{a}}_{:=u_{th}}. \quad (14)$$

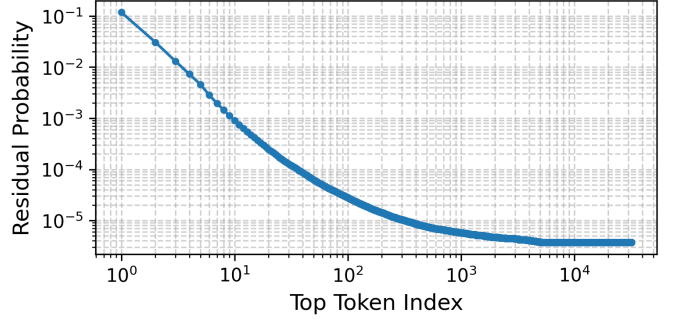
Defining $R := \int_{u=-\frac{b}{a}}^{\frac{\Delta-b}{a}} (au+b) \cdot f(u) du$ and applying Hölder's inequality to the integral yields the upper bound on R . \square

As shown in (14), we refer to setting the threshold at the upper bound as risk-prone skipping, and to using the lower bound as risk-averse skipping. The rejection risk R in **Theorem 1** quantifies the expected increase in rejection probability induced by risk-prone skipping, as determined by the uncertainty threshold and the density of the uncertainty distribution. This effectively captures the potential degradation in inference accuracy due to bypassing uplink transmission for tokens that may ultimately be rejected.

Figure 4 presents an empirical characterization of the theoretically derived uncertainty thresholds. Given $\Delta = 0.5956$ under our simulation setup, the thresholds computed from Theorem 1 are $\frac{\Delta-b}{a} = 0.8117$ for risk-prone skipping and $-\frac{b}{a} = 0.0810$ for risk-averse skipping. These thresholds are visually identified in Figure 4a, where the risk-averse threshold corresponds to the point at which the rejection probability first reaches zero—indicating that skipping occurs only for deterministically accepted tokens. Moreover, based on the empirical uncertainty distribution shown in Figure 4b, the



(a) SLM's vocabulary distribution.



(b) Residual probability with respect to top token index.

Fig. 5: (a) Average SLM vocabulary probability distribution by descending token rank (mean per rank). (b) Residual probability corresponding to the top token index, computed as the complementary cumulative distribution (i.e., $1 - \sum_{i=1}^k x_i$), where x_i denotes the probability of the k -th top-ranked token.

expected rejection risk is measured as $R = 4.94 \times 10^{-3}$, which satisfies the theoretical upper bound $R < 9.87 \times 10^{-3}$. The upper bound in (13) also suggests that a sharper slope a , induced by temperature perturbation, leads to a tighter rejection risk bound.

This empirical characterization validates the theoretical derivation and confirms its applicability to the design of the uncertainty threshold in U-HLM. By confirming the linear relationship between uncertainty and rejection probability, and validating that the rejection risk remains bounded under the derived thresholds, we establish a practical foundation for uncertainty-aware opportunistic transmission.

IV. COMPRESSED VOCABULARY TRANSMISSION FOR COMMUNICATION-EFFICIENT U-HLM

This section further presents an enhanced scheme, termed *Communication-Efficient U-HLM with Compressed Vocabulary Transmission (CU-HLM)*. In this approach, when the uncertainty exceeds the predefined threshold and uplink transmission is required, the SLM's vocabulary distribution is compressed prior to transmission to reduce communication overhead. To support this design, we analytically derive the optimal vocabulary size for both offline and online variants, based on the trade-off between token throughput and inference accuracy. The distinction between offline and online modes

lies in whether the compression process requires access to the server-side LLM's full vocabulary distribution.

A. Vocabulary Compression

To mitigate the communication bottleneck, we investigate the compressibility of the SLM's vocabulary distribution. Figure 5a illustrates the average token probability ranked in descending order, while Figure 5b shows the residual probability—defined as the cumulative probability mass of all tokens excluding the most probable ones—plotted against the number of top-ranked tokens retained.

We observe that the probability mass is heavily concentrated in a few top-ranked tokens, suggesting that the distribution can be effectively compressed if truncated appropriately. These insights support the potential applicability of vocabulary compression techniques such as top- k sampling [36].

Building on this observation, we extend our framework beyond U-HLM by incorporating a compressed vocabulary transmission scheme to further mitigate communication overhead. Specifically, when the uncertainty $u(t)$ exceeds the threshold u_{th} , the device applies a vocabulary compression method inspired by top-token sampling [36]. The idea is to transmit only a subset of the vocabulary, denoted as $\bar{\mathcal{V}} \subset \mathcal{V}$, consisting of the most probable tokens. For notational brevity, we denote the size of this compressed vocabulary as $k = |\bar{\mathcal{V}}|$.

B. Compressed Vocabulary Transmission

Given the SLM's vocabulary distribution $\mathbf{x}(t) = [x_1(t), x_2(t), \dots, x_{|\mathcal{V}|}(t)]^T$, which is sorted in descending order (i.e., $x_1(t) \geq x_2(t) \geq \dots \geq x_{|\mathcal{V}|}(t)$), the device transmits only the indices and values of the top- k tokens: $[x_1(t), x_2(t), \dots, x_k(t)]$. At the server, the LLM reconstructs the full vocabulary distribution $\hat{\mathbf{x}}(t)$ by preserving the transmitted probabilities and uniformly distributing the residual probability mass over the untransmitted tokens:

$$\hat{x}_i(t) = \begin{cases} x_i(t), & \text{for } i = 1, \dots, k, \\ \frac{1 - \sum_{i=1}^k x_i(t)}{|\mathcal{V}| - k}, & \text{for } i = k + 1, \dots, |\mathcal{V}|. \end{cases} \quad (15)$$

Despite the reconstruction in (15), distortion is introduced into the resampling distribution used in the HLM framework. We denote the resulting distorted distribution under compression as $\mathbf{q}(t)$, defined by:

$$q_v(t) = \frac{(y_v(t) - \hat{x}_v(t))^+}{\sum_i (y_i(t) - \hat{x}_i(t))^+}. \quad (16)$$

Vocabulary compression can also affect the rejection probability of the draft token, $\beta_d(t)$, thereby potentially degrading inference accuracy through two distinct mechanisms: (i) distortion of the draft token's rejection probability, and (ii) distortion of the resampling distribution as in (16). To isolate the effect of (ii), we assume that the probability and index of the draft token are always transmitted, so that its acceptance decision remains unaffected by compression.

To quantify the inference degradation induced by vocabulary compression, we revisit the unbiasedness condition in (3) and define the *bias* at round t as the total deviation between the

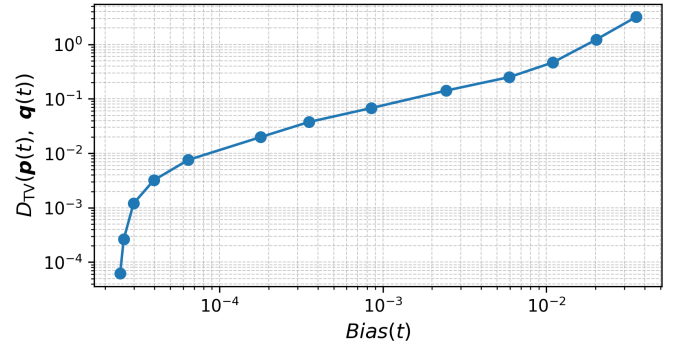


Fig. 6: Correlation between bias and the total variation distance (TVD) of the resampling distributions, evaluated across vocabulary sizes $k \in [10^0, 10^4]$.

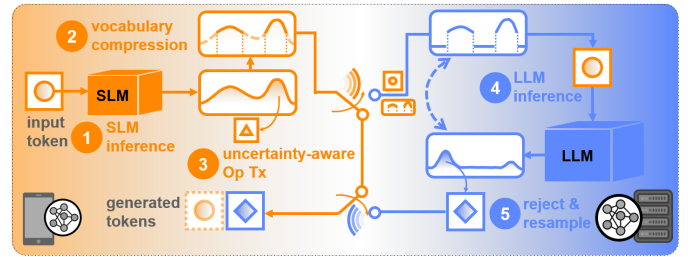


Fig. 7: Schematic illustration of CU-HLM framework. CU-HLM extends the uncertainty-aware opportunistic transmission in U-HLM by incorporating compressed vocabulary transmission for high-uncertainty tokens.

ideal hybrid inference distribution and the actual distribution under compression—to be specific, the sum of absolute differences between the LHS and RHS of (3), where the original resampling distribution $p_v(t)$ on the LHS is replaced with its distorted counterpart $q_v(t)$ under vocabulary compression:

$$\text{Bias}(t) = \sum_{v \in \mathcal{V}} \left| x_v(t)(1 - \beta_v(t)) + \left(\sum_{i \in \mathcal{V}} x_i(t)\beta_i(t) \right) q_v(t) - y_v(t) \right|. \quad (17)$$

To simplify the analysis, we define the total variation distance (TVD) between the original and distorted resampling distributions to quantify distortion introduced solely in the resampling step:

$$D_{TV}(\mathbf{p}(t), \mathbf{q}(t)) = \frac{1}{2} \sum_i |p_i(t) - q_i(t)|. \quad (18)$$

Empirical analysis (Figure 6) reveals a strong linear correlation between TVD and bias $\text{Bias}(t)$, with a correlation coefficient of 0.9763. This observation justifies the use of TVD as a surrogate for bias and thus a reliable proxy for inference accuracy. Since uplink communication cost increases linearly with the number of transmitted tokens, as shown in (4), we aim to determine the smallest compressed vocabulary size that satisfies a bounded TVD constraint. This leads to the following optimization problem:

$$k(t)^* = \arg \min_{k(t)} \{k(t) \mid D_{TV}(\mathbf{p}(t), \mathbf{q}(t)) \leq \theta\}, \quad (19)$$

Algorithm 1 Operational flow of CU-HLM.

Require: Input token sequence \mathbf{s} , u_{th} , $k(t)^* \forall t$, r_{max} , θ_{max}

- 1: **while** $|\mathbf{r}(t-1)| < r_{\text{max}}$ **and** $r(t-1) \neq \text{EOS}$ **do**
- 2: **// SLM Operation at Device (Round t)**
- 3: Generate input $\mathbf{s}(t) = \mathbf{s} \oplus \mathbf{r}(t-1)$
- 4: Sample $\{\theta^{(1)}, \dots, \theta^{(M)}\}$ from $[0, \theta_{\text{max}}]$
- 5: Generate vocabulary distributions $\mathbf{x}(t)$, $\tilde{\mathbf{x}}^{(m)}(t) \forall m$
- 6: Sample draft token d and perturbed tokens $d^{(m)} \forall m$
- 7: Measure uncertainty $u(t)$ via (9)
- 8: Set $r(t) \leftarrow d$
- 9: **if** $u(t) > u_{\text{th}}$ **then**
- 10: Upload top $k(t)^*$ tokens $\{x_1(t), \dots, x_{k(t)^*}(t)\}$ and draft token d to the BS
- 11: **// LLM Operation at BS (Round t)**
- 12: Reconstruct full distribution $\hat{\mathbf{x}}(t)$ via (15)
- 13: Generate LLM distribution $\mathbf{y}(t)$ by processing $\mathbf{s}(t)$
- 14: **if** $y_d(t) < x_d(t)$ **then**
- 15: With probability $1 - \frac{y_d(t)}{x_d(t)}$, sample a target token $r(t) = d^*$ from:

$$P(r(t) = d^*) = \frac{(y_{d^*}(t) - \hat{x}_{d^*}(t))^+}{\sum_{i=1}^{|\mathcal{V}|} (y_i(t) - \hat{x}_i(t))^+}$$
- 16: **end if**
- 17: Send $r(t)$ to the device
- 18: **else if** $u(t) \leq u_{\text{th}}$ **then**
- 19: **Opportunistic Skipping**
- 20: **end if**
- 21: Update $\mathbf{r}(t) = \mathbf{r}(t-1) \oplus r(t)$, $t \leftarrow t + 1$
- 22: **end while**

where θ denotes the maximum tolerable distortion.

To implement the above optimization in practice, we design two variations of CU-HLM that differ in how they set the vocabulary compression level. The first is an *offline* approach, which selects a static compression strategy using time-averaged statistical information and applies it throughout all rounds. The second is an *online* approach, which dynamically adjusts the compression level at each round using only time-varying information available on the device, without requiring access to stochastic distributions or prior statistics.

The complete procedure of CU-HLM is summarized in **Algorithm 1** and illustrated in Figure 7, describing its extended operation beyond U-HLM through the integration of compressed vocabulary transmission.

C. Offline Vocabulary Compression

Directly computing $D_{\text{TV}}(\mathbf{p}(t), \mathbf{q}(t))$ is computationally expensive, as it involves accessing the full LLM distribution $y_v(t)$, computing the resampling distributions in (2) and (16), and evaluating their element-wise difference. To improve tractability, we instead derive the following upper bound:

Proposition 1 (Upper Bound on Total Variation Distance). *Given that $\mathbf{x}(t)$ and $\mathbf{y}(t)$ denote the vocabulary distributions of the SLM and LLM at the t -th round, respectively, the total*

variation distance between the resampling distributions $\mathbf{p}(t)$ and $\mathbf{q}(t)$ is upper bounded as:

$$D_{\text{TV}}(\mathbf{p}(t), \mathbf{q}(t)) \leq \underbrace{\frac{\sum_{i=k+1}^{|\mathcal{V}|} |x_i(t) - \hat{x}_i(t)|}{D_{\text{TV}}(\mathbf{x}(t), \mathbf{y}(t))}}_{:= U_{\text{TV}}(k, t)}. \quad (20)$$

Proof. See Appendix A. \square

This upper bound offers a tractable approximation of the TVD, enabling efficient estimation of resampling distortion without requiring full computation. Note, however, that $U_{\text{TV}}(k, t)$ depends on the full LLM-side distribution $\mathbf{y}(t)$, which is not accessible at the device side. To address this, we assume access to a statistical estimate of the long-term average of $U_{\text{TV}}(k, t)$, which can be practically obtained via periodic downlink feedback from the server sharing historical observations of $\mathbf{y}(t)$.

Remark 2 (Offline Vocabulary Compression). *We determine a fixed compressed vocabulary size k^* that minimizes uplink communication cost while ensuring that the resampling distortion remains within a specified tolerance θ . This is achieved by replacing the per-round constraint in (19) with a time-averaged upper bound $\mathbb{E}_t[U_{\text{TV}}(k, t)]$, leading to the following relaxed optimization:*

$$k^* = \arg \min_k \{k \mid \mathbb{E}_t[U_{\text{TV}}(k, t)] \leq \theta\}. \quad (21)$$

This approach is effective for offline tuning, but its applicability is limited in online contexts, as k^* is fixed across all rounds t . Future work may explore tighter theoretical bounds using known inequalities that relate TVD to Wasserstein distance [37] or Kullback–Leibler divergence [38], [39].

D. Online Vocabulary Compression

To overcome the limitations of offline compression and support real-time deployment, we now propose an online vocabulary compression scheme that can be executed entirely on-device without requiring any server-side feedback.

We begin by approximating the denominator of $U_{\text{TV}}(k, t)$ —specifically, the TVD $D_{\text{TV}}(\mathbf{x}(t), \mathbf{y}(t))$ —as follows:

$$\begin{aligned} D_{\text{TV}}(\mathbf{x}(t), \mathbf{y}(t)) &\stackrel{(a)}{=} \sum_{i=1}^{|\mathcal{V}|} x_i(t) \left(\frac{y_i(t)}{x_i(t)} - 1 \right)^+ \\ &\stackrel{(b)}{\approx} \sum_{i=1}^{|\mathcal{V}|} x_i(t) \cdot \ell \left(\frac{y_i(t)}{x_i(t)} - 1 \right), \end{aligned} \quad (22)$$

where $\ell(z) := \frac{\ln(1+e^{\eta z})}{\eta}$ denotes the softplus function with temperature parameter η . Step (a) is valid since $x_i(t) > 0$ from the softmax in (1), and (b) uses a smooth approximation of the ReLU function [40].

The maximum error of this approximation is bounded by $\ln 2/\eta$, occurring at $z = 0$, i.e., when $y_i(t) = x_i(t)$ (zero rejection). Since such cases are skipped under U-HLM, the approximation error is negligible for moderate values of η .

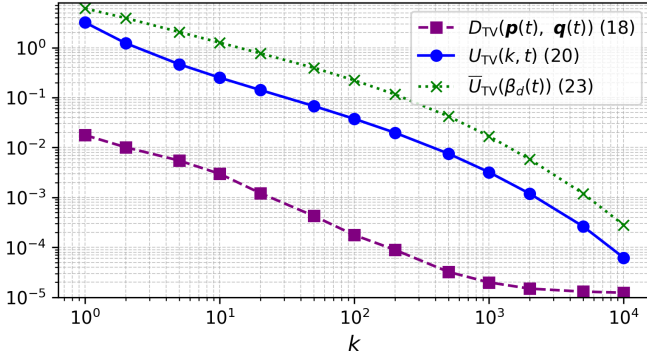


Fig. 8: Comparison of TVD and its upper bounds w.r.t. k .

We define $\hat{U}_{TV}(k, t)$ as an approximate form of $U_{TV}(k, t)$, where the denominator $D_{TV}(\mathbf{x}(t), \mathbf{y}(t))$ is replaced by its approximated counterpart in (22). We now present an upper bound on this term:

Proposition 2 (Approximated Upper Bound on $U_{TV}(k, t)$). *The approximated TVD $\hat{U}_{TV}(k, t)$ is upper bounded as:*

$$\hat{U}_{TV}(k, t) < \underbrace{\frac{\sum_{i=k+1}^{|\mathcal{V}|} |x_i(t) - \hat{x}_i(t)|}{(1 - x_d(t)) \cdot \ell(-1) + x_d(t) \cdot \ell(-\beta_d(t))}}_{:= \bar{U}_{TV}(\beta_d(t))}. \quad (23)$$

Proof. See Appendix B. \square

All components of $\bar{U}_{TV}(\beta_d(t))$ —namely $x_d(t)$, $\beta_d(t)$, and $\sum_{i=k+1}^{|\mathcal{V}|} |x_i(t) - \hat{x}_i(t)|$ —are either directly observable or locally computable on the device. In particular, $\beta_d(t)$ is estimated from the token’s uncertainty using the linear model in (7). This enables fully on-device, token-level vocabulary compression without requiring server-side information.

Remark 3 (Uncertainty-Aware Online Vocabulary Compression). *We propose an online vocabulary compression scheme that selects the compressed vocabulary size at each round t as:*

$$k(t)^* = \arg \min_{k(t)} \{k(t) \mid \bar{U}_{TV}(a u(t) + b) \leq \theta\}. \quad (24)$$

The goal is to minimize the instantaneous uplink payload while ensuring that the estimated resampling distortion remains within the tolerance θ . This formulation serves as a relaxed version of the original problem in (19), where the intractable constraint on D_{TV} is approximated using observable, uncertainty-based quantities.

Since $\bar{U}_{TV}(\beta_d(t))$ increases with $\beta_d(t)$, the resulting vocabulary size $k(t)^*$ naturally grows with uncertainty, thereby allocating higher transmission fidelity to more uncertain tokens.

We note that both bounds $U_{TV}(k, t)$ and $\bar{U}_{TV}(\beta_d(t))$ share the same numerator—dependent on the residual mass beyond the top- k tokens—and differ only in their denominator formulations. As a result, both bounds exhibit similar decreasing trends as the compressed vocabulary size k increases. As shown in Figure 8, $U_{TV}(k, t)$ provides a tight upper bound on

the actual TVD, while $\bar{U}_{TV}(\beta_d(t))$ also becomes increasingly accurate with larger vocabulary sizes, despite relying only on local information.

While both the offline and online designs aim to minimize communication under a fixed distortion constraint, our framework can be extended to the dual objective—maximizing inference accuracy under a communication budget—which we leave for future work. Lastly, although our analysis is based on top-ranked token selection, the proposed vocabulary size adaptation strategy can be extended to threshold-based methods such as top- p (nucleus) sampling [41] and min- p sampling [42], using conversion rules outlined in [43].

These results lay the groundwork for the offline and online vocabulary compression strategies in CU-HLM. Through tractable upper bound formulations and corresponding policy designs, we are equipped to empirically evaluate their effectiveness in the subsequent experiments.

V. NUMERICAL EVALUATION

This section presents experimental results validating the effectiveness of the proposed CU-HLM framework, including both its online and offline vocabulary compression schemes. We begin by detailing the simulation setup and evaluation metrics, followed by a comprehensive analysis of the results.

A. Simulation Setup

Unless otherwise specified, all experiments are conducted using TinyLlama-1.1B as the SLM and Llama2-13B as the LLM, with a vocabulary size of $|\mathcal{V}| = 32,000$. The Alpaca dataset [44] is employed as the benchmark, with a fixed set of 100 randomly selected samples used across all experiments. All simulations are performed on a Linux-based server equipped with an 8-core Intel Xeon Silver 4215R CPU and three Nvidia GeForce RTX 3090 GPUs. Under this setup, the average per-token wall time is measured as $\tau_{SLM} = 25.6$ ms and $\tau_{LLM} = 104.6$ ms.

We evaluate the proposed CU-HLM framework—both with online and offline vocabulary compression—alongside U-HLM, and compare them against several baselines: (i) LLM-only inference, (ii) SLM-only inference, (iii) the original HLM, and (iv) Rand-HLM, which skips uplink transmissions at random with a fixed probability of 0.5. The performance is evaluated using the following metrics:

- **Inference Accuracy:** Measured as the cosine similarity between sentence embeddings of the generated response and the corresponding ground-truth answer, where embeddings are computed using a BERT model [45].
- **Token Throughput:** Defined as the average number of tokens generated per second over the full sequence, extended from the per-round throughput defined in (6).

The remaining hyperparameters are configured as: uplink bandwidth $W = 10$ MHz, $b_{\text{prob}} = 8$, and $r_{\text{max}} = 512$.

B. Impact of Design Parameters on Accuracy and communication efficiency

Before evaluating the overall performance of CU-HLM, this subsection investigates the empirical impact of its two

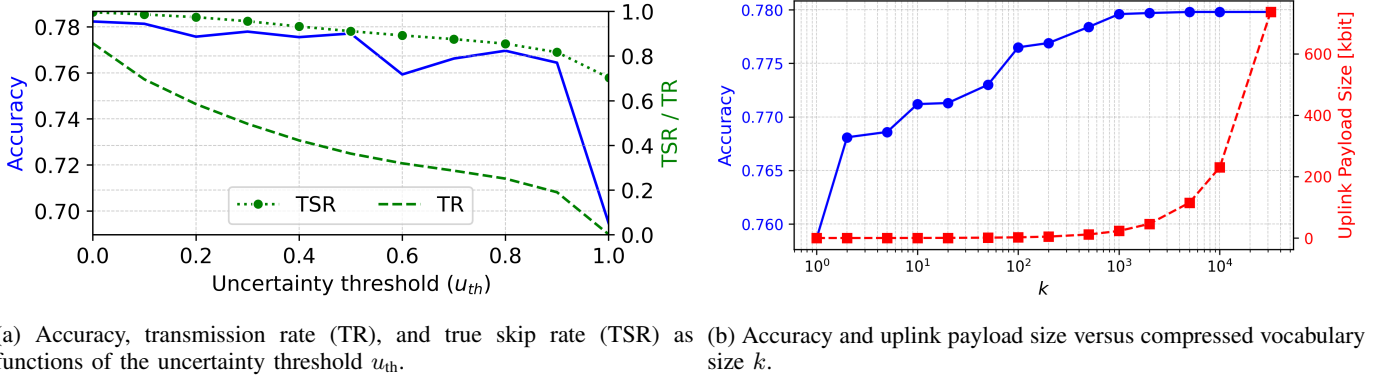


Fig. 9: Accuracy and communication efficiency with respect to design parameters in CU-HLM.

key hyperparameters—namely, the uncertainty threshold and the compressed vocabulary size—on inference accuracy and communication efficiency. Based on this analysis, we finalize the parameter settings for subsequent experiments.

To begin, we assess the effect of the uncertainty threshold u_{th} using the following two metrics:

- **Transmission Rate (TR):** The proportion of rounds in which an uplink transmission occurs. In standard HLM, this defaults to 1 and serves as an indicator of communication efficiency.
- **True Skip Rate (TSR):** The probability that a skipped token is eventually accepted by the LLM, used to assess the accuracy impact of skipping.

Figure 9a shows that increasing u_{th} leads to a decrease in both TR and TSR. A higher threshold makes the model more aggressive in skipping, thereby reducing the frequency of uplink transmissions (lower TR). However, this also increases the likelihood of skipping tokens that would have been rejected (lower TSR). Fortunately, the drop in TSR is relatively moderate—remaining above 0.702—even at high thresholds. This resilience can be attributed to the distribution of uncertainty values, which is concentrated near the extremes (0 and 1), as shown in Figure 4b. This implies that raising u_{th} still preserves a significant portion of accurate skips.

As a result, inference accuracy also tends to decrease with increasing u_{th} , but remains well-preserved up to a certain point. Notably, two inflection points in the accuracy curve are observed, with the most significant drop occurring at $u_{th} = 0.9$. This aligns well with the risk-prone threshold of 0.8117 derived in **Theorem 1**, thereby validating the theoretical analysis. For the uncertainty threshold, we set $u_{th} = 0.8$, which allows the model to skip uplink transmissions for approximately 74.8% of tokens.

Figure 9b illustrates the trade-off between inference accuracy and uplink payload size with respect to the compressed vocabulary size k . As expected, increasing k improves accuracy while linearly increasing communication cost, showing a clear monotonic trend in both metrics. Based on these empirical observations, and considering the trade-off between communication efficiency and accuracy, we fix the tolerance parameter as $\theta = 0.1$, which yields an offline vocabulary size of $k^* = 30$. This corresponds to less than 0.1% of the full

vocabulary size in terms of uplink payload.

It is worth noting that the reported uplink payload size represents a worst-case estimate, indicating room for further optimization in both communication and computation. On the communication side, advanced compression techniques—such as source coding based on token-wise entropy within the vocabulary—could further reduce the transmission cost. On the computation side, our analysis does not yet account for potential runtime savings that may result from operating on smaller values of k , which could further improve overall system efficiency.

C. Inference Accuracy and Token Throughput Comparison

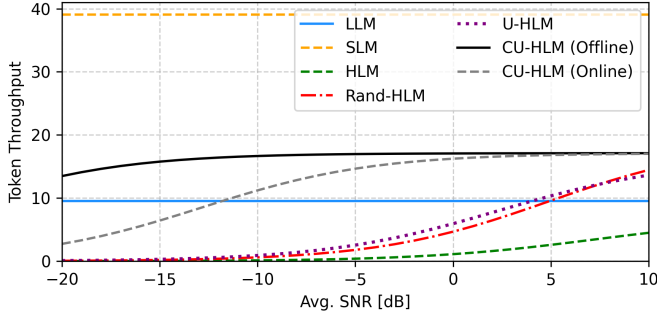
This subsection presents the overall performance of CU-HLM by jointly assessing the impact of previously discussed components. Table I evaluates inference accuracy across multiple model configurations and datasets—including QED, CREAK, and StrategyQA from the FLAN collection [46]—while extending the evaluation to include Llama2-7B as the LLM. Figure 10 further illustrates token throughput across different inference methods under two wireless fading environments: Rayleigh and Rician (with $K = 10$ dB), across average SNRs ranging from -20 to 10 dB.

We first note that HLM, LLM, and SLM serve as upper bounds in terms of inference accuracy and token throughput, as observed in both Table I and Figure 10. In general, better channel conditions—i.e., higher SNR and under a Rician fading channel—lead to improved token throughput, as demonstrated in Figure 10a and Figure 10b. Within this context, U-HLM outperforms Rand-HLM by consistently achieving higher inference accuracy at similar token throughput levels, demonstrating the efficacy of uncertainty-based opportunistic transmission.

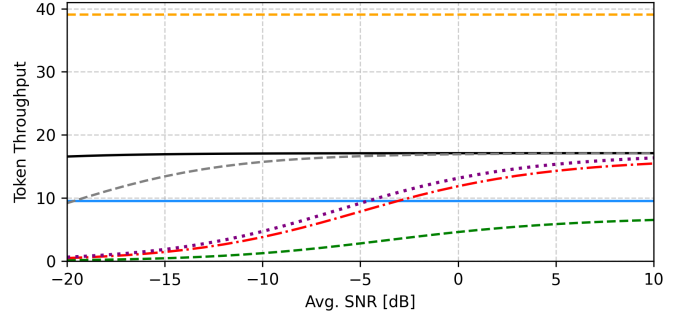
Next, we analyze CU-HLM with offline and online vocabulary compression. Compared to standard HLM inference, CU-HLM significantly improves token throughput while maintaining competitive accuracy. For instance, on the Alpaca dataset with Llama2-13B, CU-HLM achieves inference accuracy of 96.91% (offline) and 97.42% (online). The token throughput gains are consistently observed across various fading channels and SNRs. As shown in Figure 10a, the improvement is particularly significant under Rayleigh fading with an average

TABLE I: Comparison of inference accuracy across different methods, SLM–LLM pairs, and datasets.

Inference Method	TinyLlama 1.1B – Llama2 13B				TinyLlama 1.1B – Llama2 7B			
	Alpaca	QED	CREAK	StrategyQA	Alpaca	QED	CREAK	StrategyQA
LLM	0.7782	0.6954	0.6722	0.7122	0.7758	0.6271	0.6621	0.6779
SLM	0.6941	0.5139	0.5291	0.5694	0.6521	0.5139	0.5291	0.5694
HLM	0.7825	0.7226	0.6946	0.6983	0.7823	0.6517	0.6529	0.6883
Rand-HLM	0.7385	0.6128	0.6406	0.6227	0.7382	0.5534	0.5682	0.6200
U-HLM	0.7704	0.7122	0.6854	0.6844	0.7696	0.6381	0.6550	0.6532
CU-HLM (Offline)	0.7583	0.6713	0.6508	0.6773	0.7455	0.6130	0.6062	0.6242
CU-HLM (Online)	0.7623	0.6876	0.6672	0.6817	0.7622	0.6387	0.6460	0.6409



(a) Rayleigh fading channel.



(b) Rician fading channel with a K-factor of 10 dB.

Fig. 10: Token throughput across inference methods as a function of average SNR under different fading conditions.

SNR of -20 dB, where CU-HLM achieves up to $1014.1\times$ (offline) and $206\times$ (online) throughput gains. These gains are primarily attributed to the uncertainty-aware opportunistic and compressed transmission, which substantially reduces both uplink transmit opportunity and payload size.

The accuracy–throughput trade-off between the offline and online variants of CU-HLM arises from differences in the tightness of their respective compression bounds. CU-HLM (Offline) employs a fixed compressed vocabulary size of $k^* = 30$, whereas CU-HLM (Online) dynamically adjusts $k(t)^*$ between 4 and 5,715 (averaging 832, i.e., only 2.6% of the full vocabulary) based on the estimated rejection probability and $x_d(t)$, as defined in (23). While the bound used in CU-HLM (Online) is looser, its ability to dynamically select near-optimal compression levels allows it to achieve token throughput comparable to its offline counterpart under moderate SNR conditions. However, under extremely low-SNR regimes, CU-HLM (Offline), which leverages server-side information, yields more stable gains, though the gap diminishes as the SNR increases and channel quality improves.

Taken together, the results in Table I and Figure 10 demonstrate that CU-HLM offers a favorable balance between inference accuracy and communication efficiency. It generalizes well across diverse datasets, model configurations, and wireless channel conditions. The online variant operates solely on on-device information without statistical feedback, yet achieves performance comparable to the offline variant, which leverages tighter, feedback-assisted compression.

TABLE II: Latency breakdown and token throughput of U-HLM and CU-HLM (Online) under different configurations, measured under Rayleigh fading with average SNR = 10 dB. SLM computation time is fixed at 25.6 ms (64 ms for 7B–13B*), and all values reflect average latency per token.

Method	Communication	LLM Computation	Token Throughput
<i>Baseline: U-HLM</i>			
+ No KD	6.3 ms	31.1 ms	15.9
+ KD	5.9 ms	29.0 ms	16.5
+ 7B–13B*	2.8 ms	13.8 ms	12.4
<i>CU-HLM (Online)</i>			
+ No KD	38.1 μ s	30.0 ms	18.0
+ KD	35.5 μ s	27.9 ms	18.7
+ 7B–13B*	16.2 μ s	12.8 ms	13.0

D. Ablation Study: Impact of SLM Architecture and Alignment

The token throughput of CU-HLM is fundamentally influenced by how well the SLM’s predictions align with those of the LLM. While CU-HLM significantly reduces uplink communication latency through uncertainty-aware skipping and compression, the LLM computation latency remains a dominant bottleneck, as shown in Table II. To examine whether improved SLM behavior can further alleviate this issue, we evaluate two variations designed to enhance either the SLM architecture or its alignment with the LLM. For architectural improvement, we replace the default SLM with a larger 7B model. For alignment, we fine-tune the SLM using knowledge distillation (KD), where the LLM (Llama2-13B) provides soft targets in the form of output logits.

Experiments under Rayleigh fading with 10 dB SNR show that both strategies raise acceptance rates and reduce LLM invocation. KD yields a modest 2% increase in acceptance, translating to a 7% reduction in LLM latency without increasing SLM computation time. The larger SLM achieves a 16.5% acceptance gain but incurs over 150% higher SLM computation latency, offsetting part of the benefit. These results confirm that both architectural capacity and alignment quality contribute to acceptance rates, and thus token throughput, with distinct trade-offs. Among the two, KD provides a lightweight yet effective improvement, and may be further extended to training-time integration [47] or applied alongside sparse transfer techniques [48]. We leave this direction as promising future work.

VI. CONCLUSION

This paper presents CU-HLM, a communication-efficient hybrid language model framework tailored for wireless edge inference. By leveraging the strong empirical correlation between token-level uncertainty and rejection probability, we develop an uncertainty-aware opportunistic transmission mechanism that selectively skips both uplink communication and LLM computation for low-uncertainty tokens. To further reduce communication overhead under high uncertainty, we introduce a compressed vocabulary transmission scheme and analytically formulate the optimal compression policy for both offline and online deployment scenarios. Extensive experiments across diverse datasets, model configurations, and wireless channel conditions confirm that CU-HLM substantially enhances communication efficiency while maintaining near-LLM inference accuracy. These results highlight CU-HLM's potential as a scalable solution for efficient on-device language modeling in bandwidth-constrained environments. Future work includes extending our approach to heterogeneous multi-agent systems built upon A2A [49] and MCP [50] protocols, where agents differ in capability, context access, and model capacity.

APPENDIX A PROOF OF PROPOSITION 1

We begin by recalling the definition of the TVD between two probability distributions $\mathbf{p}(t)$ and $\mathbf{q}(t)$ as

$$D_{\text{TV}}(\mathbf{p}(t), \mathbf{q}(t)) = \frac{1}{2} \|\mathbf{p}(t) - \mathbf{q}(t)\|_1, \quad (25)$$

where $\|\cdot\|_1$ denotes the ℓ_1 -norm, defined as the sum of the absolute values of the vector's components.

To simplify the analysis, define two auxiliary vectors $\boldsymbol{\gamma}$ and $\boldsymbol{\omega}$ such that the v -th components are given by $\gamma_v = (y_v(t) - x_v(t))^+$ and $\omega_v = (y_v(t) - \hat{x}_v(t))^+$, respectively.

Substituting these into (25), we have:

$$D_{\text{TV}}(\mathbf{p}(t), \mathbf{q}(t)) = \frac{1}{2} \left\| \frac{\boldsymbol{\gamma}}{\|\boldsymbol{\gamma}\|_1} - \frac{\boldsymbol{\omega}}{\|\boldsymbol{\omega}\|_1} \right\|_1. \quad (26)$$

We decompose the ℓ_1 -norm as follows:

$$\begin{aligned} \left\| \frac{\boldsymbol{\gamma}}{\|\boldsymbol{\gamma}\|_1} - \frac{\boldsymbol{\omega}}{\|\boldsymbol{\omega}\|_1} \right\|_1 &= \left\| \left(\frac{\boldsymbol{\gamma}}{\|\boldsymbol{\gamma}\|_1} - \frac{\boldsymbol{\omega}}{\|\boldsymbol{\gamma}\|_1} \right) + \left(\frac{\boldsymbol{\omega}}{\|\boldsymbol{\gamma}\|_1} - \frac{\boldsymbol{\omega}}{\|\boldsymbol{\omega}\|_1} \right) \right\|_1 \\ &\stackrel{(a)}{\leq} \left\| \frac{\boldsymbol{\gamma} - \boldsymbol{\omega}}{\|\boldsymbol{\gamma}\|_1} \right\|_1 + \left\| \boldsymbol{\omega} \left(\frac{1}{\|\boldsymbol{\gamma}\|_1} - \frac{1}{\|\boldsymbol{\omega}\|_1} \right) \right\|_1, \end{aligned} \quad (28)$$

where (a) follows from the triangle inequality.

We now bound each term separately. For the first term:

$$\left\| \frac{\boldsymbol{\gamma} - \boldsymbol{\omega}}{\|\boldsymbol{\gamma}\|_1} \right\|_1 = \frac{\|\boldsymbol{\gamma} - \boldsymbol{\omega}\|_1}{\|\boldsymbol{\gamma}\|_1}. \quad (29)$$

For the second term, using the reverse triangle inequality:

$$\begin{aligned} \left\| \boldsymbol{\omega} \left(\frac{1}{\|\boldsymbol{\gamma}\|_1} - \frac{1}{\|\boldsymbol{\omega}\|_1} \right) \right\|_1 &= \|\boldsymbol{\omega}\|_1 \cdot \left| \frac{1}{\|\boldsymbol{\gamma}\|_1} - \frac{1}{\|\boldsymbol{\omega}\|_1} \right| \\ &= \frac{|\|\boldsymbol{\gamma}\|_1 - \|\boldsymbol{\omega}\|_1|}{\|\boldsymbol{\gamma}\|_1} \\ &\leq \frac{\|\boldsymbol{\gamma} - \boldsymbol{\omega}\|_1}{\|\boldsymbol{\gamma}\|_1}. \end{aligned} \quad (30)$$

Thus, combining (29) and (30), we obtain:

$$D_{\text{TV}}(\mathbf{p}(t), \mathbf{q}(t)) \leq \frac{\|\boldsymbol{\gamma} - \boldsymbol{\omega}\|_1}{\|\boldsymbol{\gamma}\|_1}. \quad (31)$$

Next, we bound the numerator. Since ReLU is a 1-Lipschitz function, it holds that:

$$\begin{aligned} \|\boldsymbol{\gamma} - \boldsymbol{\omega}\|_1 &\leq \|\mathbf{x}(t) - \hat{\mathbf{x}}(t)\|_1 \\ &= \|(\mathbf{x}(t) - \hat{\mathbf{x}}(t))_{k+1:|\mathcal{V}|}\|_1, \end{aligned} \quad (32)$$

where $(\cdot)_{a:b}$ denotes the subvector consisting of indices from a to b , exploiting the fact that $\mathbf{x}(t)$ and $\hat{\mathbf{x}}(t)$ are identical over the top- k elements.

Finally, for the denominator, since both $\mathbf{x}(t)$ and $\mathbf{y}(t)$ are valid probability distributions, we apply mass conservation to obtain:

$$\|\boldsymbol{\gamma}\|_1 = \sum_{i=1}^{|\mathcal{V}|} (y_i(t) - x_i(t))^+ \quad (33)$$

$$= \frac{1}{2} \sum_{i=1}^{|\mathcal{V}|} |y_i(t) - x_i(t)| = D_{\text{TV}}(\mathbf{x}(t), \mathbf{y}(t)). \quad (34)$$

Substituting (32) and (34) completes the proof. \square

APPENDIX B PROOF OF PROPOSITION 2

From the approximation in (22), we decompose the sum into the draft token and the non-draft tokens as:

$$\begin{aligned} \sum_{i=1}^{|\mathcal{V}|} x_i(t) \cdot \ell \left(\frac{y_i(t)}{x_i(t)} - 1 \right) &= x_d(t) \cdot \ell \left(\frac{y_d(t)}{x_d(t)} - 1 \right) \\ &\quad + \sum_{i \neq d} x_i(t) \cdot \ell \left(\frac{y_i(t)}{x_i(t)} - 1 \right). \end{aligned} \quad (35)$$

Since $\ell(z)$ is monotonically increasing and both $x_i(t)$ and $y_i(t)$ are outputs of softmax operations (thus strictly positive for all $i \in \mathcal{V}$), we separately bound the draft and non-draft terms as follows.

For the draft token term, we have:

$$\begin{aligned} \ell \left(\frac{y_d(t)}{x_d(t)} - 1 \right) &= \ell \left(- \left(1 - \frac{y_d(t)}{x_d(t)} \right) \right) \\ &\geq \ell \left(- \left(1 - \frac{y_d(t)}{x_d(t)} \right)^+ \right) \\ &= \ell(-\beta_d(t)), \end{aligned} \quad (36)$$

where the inequality follows because $\ell(z)$ is increasing and $\left(1 - \frac{y_d(t)}{x_d(t)}\right) \leq \left(1 - \frac{y_d(t)}{x_d(t)}\right)^+$. Next, for each non-draft token $i \neq d$, since $y_i(t) > 0$ and $x_i(t) > 0$, we have:

$$\ell\left(\frac{y_i(t)}{x_i(t)} - 1\right) > \ell(-1). \quad (37)$$

Combining the two bounds, the denominator in Proposition 2 is lower-bounded by

$$x_d(t) \cdot \ell(-\beta_d(t)) + (1 - x_d(t)) \cdot \ell(-1).$$

Substituting this into the denominator of $\hat{U}_{TV}(k, t)$ yields the desired upper bound, completing the proof. \square

REFERENCES

- [1] J. Hoffmann et al., “Training compute-optimal large language models,” *arXiv preprint arXiv:2203.15556*, 2022.
- [2] A. Chowdhery, S. Narang, J. Devlin, M. Bosma, G. Mishra, A. Roberts, et al., “Palm: Scaling language modeling with pathways,” *Journal of Machine Learning Research*, vol. 24, no. 240, pp. 1–113, 2023.
- [3] A. J. Thirunavukarasu, D. S. J. Ting, K. Elangovan, L. Gutierrez, T. F. Tan, and D. S. W. Ting, “Large language models in medicine,” *Nature medicine*, vol. 29, no. 8, pp. 1930–1940, 2023.
- [4] D. Demszky, D. Yang, D. S. Yeager, C. J. Bryan, M. Clapper, S. Chandhok, et al., “Using large language models in psychology,” *Nature Reviews Psychology*, vol. 2, no. 11, pp. 688–701, 2023.
- [5] W. X. Zhao, K. Zhou, J. Li, T. Tang, X. Wang, Y. Hou, et al., “A survey of large language models,” *arXiv preprint arXiv:2303.18223*, 2023.
- [6] J. Yang et al., “Harnessing the power of llms in practice: A survey on chatgpt and beyond,” *ACM KDD*, vol. 18, no. 6, pp. 1–32, 2024.
- [7] Z. Hao, H. Jiang, S. Jiang, J. Ren, and T. Cao, “Hybrid slm and llm for edge-cloud collaborative inference,” in *Proceedings of the Workshop on Edge and Mobile Foundation Models*, pp. 36–41, 2024.
- [8] Y. Leviathan, M. Kalman, and Y. Matias, “Fast inference from transformers via speculative decoding,” in *International Conference on Machine Learning*, pp. 19274–19286, PMLR, 2023.
- [9] H. Touvron, T. Lavril, G. Izacard, X. Martinet, M.-A. Lachaux, T. Lacroix, et al., “Llama: Open and efficient foundation language models,” *arXiv preprint arXiv:2302.13971*, 2023.
- [10] G. Team, T. Mesnard, C. Hardin, R. Dadashi, S. Bhupatiraju, S. Pathak, et al., “Gemma: Open models based on gemini research and technology,” *arXiv preprint arXiv:2403.08295*, 2024.
- [11] D. Guo, D. Yang, H. Zhang, J. Song, R. Zhang, R. Xu, et al., “Deepseek-r1: Incentivizing reasoning capability in llms via reinforcement learning,” *arXiv preprint arXiv:2501.12948*, 2025.
- [12] K. Zhang, J. Wang, N. Ding, B. Qi, E. Hua, X. Lv, and B. Zhou, “Fast and slow generating: An empirical study on large and small language models collaborative decoding,” *arXiv preprint arXiv:2406.12295*, 2024.
- [13] S. V. Kandala, P. Medaranga, and A. Varshney, “Tinyllm: A framework for training and deploying language models at the edge computers,” *arXiv preprint arXiv:2412.15304*, 2024.
- [14] P. Zhang, G. Zeng, T. Wang, and W. Lu, “Tinyllama: An open-source small language model,” *arXiv preprint arXiv:2401.02385*, 2024.
- [15] M. Javaheripi, S. Bubeck, M. Abidin, J. Aneja, S. Bubeck, C. C. T. Mendes, et al., “Phi-2: The surprising power of small language models,” *Microsoft Research Blog*, vol. 1, no. 3, p. 3, 2023.
- [16] X. Chu, L. Qiao, X. Zhang, S. Xu, F. Wei, Y. Yang, et al., “Mobilevlm v2: Faster and stronger baseline for vision language model,” *arXiv preprint arXiv:2402.03766*, 2024.
- [17] P. P. Ray and M. P. Pradhan, “Llmedge: A novel framework for localized llm inferencing at resource constrained edge,” in *2024 International Conference on IoT Based Control Networks and Intelligent Systems (ICICNIS)*, pp. 1–8, IEEE, 2024.
- [18] X. Ma, G. Fang, and X. Wang, “Llm-pruner: On the structural pruning of large language models,” *Advances in neural information processing systems*, vol. 36, pp. 21702–21720, 2023.
- [19] Y. Li et al., “Loftq: Lora-fine-tuning-aware quantization for large language models,” *arXiv preprint arXiv:2310.08659*, 2023.
- [20] Y. Zhou, K. Lyu, A. S. Rawat, A. K. Menon, A. Rostamizadeh, S. Kumar, et al., “Distillspec: Improving speculative decoding via knowledge distillation,” *arXiv preprint arXiv:2310.08461*, 2023.
- [21] W. Wang, W. Chen, Y. Luo, Y. Long, Z. Lin, L. Zhang, et al., “Model compression and efficient inference for large language models: A survey,” *arXiv preprint arXiv:2402.09748*, 2024.
- [22] D. Xu, W. Yin, X. Jin, Y. Zhang, S. Wei, M. Xu, and X. Liu, “Llmcd: Fast and scalable on-device large language model inference,” *arXiv preprint arXiv:2309.04255*, 2023.
- [23] J. She, W. Zheng, Z. Liu, H. Wang, E. Xing, H. Yao, and Q. Ho, “Token level routing inference system for edge devices,” *arXiv preprint arXiv:2504.07878*, 2025.
- [24] D. Xu, W. Yin, H. Zhang, X. Jin, Y. Zhang, S. Wei, M. Xu, and X. Liu, “Edgellm: Fast on-device llm inference with speculative decoding,” *IEEE Transactions on Mobile Computing*, 2024.
- [25] C. Chen, S. Borgeaud, G. Irving, J.-B. Lespiau, L. Sifre, and J. Jumper, “Accelerating large language model decoding with speculative sampling,” *arXiv preprint arXiv:2302.01318*, 2023.
- [26] Z. Yu, Z. Wang, Y. Li, R. Gao, X. Zhou, S. R. Bommur, Y. Zhao, and Y. Lin, “Edge-llm: Enabling efficient large language model adaptation on edge devices via unified compression and adaptive layer voting,” in *Proceedings of the 61st ACM/IEEE Design Automation Conference*, pp. 1–6, 2024.
- [27] M. Huang, A. Shen, K. Li, H. Peng, B. Li, and H. Yu, “Edgellm: A highly efficient cpu-fpga heterogeneous edge accelerator for large language models,” *arXiv preprint arXiv:2407.21325*, 2024.
- [28] S. Shi, E. Zhao, D. Cai, L. Cui, X. Huang, and H. Li, “Inferflow: an efficient and highly configurable inference engine for large language models,” *arXiv preprint arXiv:2401.08294*, 2024.
- [29] Y. Wang, K. Chen, H. Tan, and K. Guo, “Tabi: An efficient multi-level inference system for large language models,” in *Proceedings of the Eighteenth European Conference on Computer Systems*, pp. 233–248, 2023.
- [30] W. Zheng, Y. Chen, W. Zhang, S. Kundu, Y. Li, Z. Liu, E. P. Xing, H. Wang, and H. Yao, “Citer: Collaborative inference for efficient large language model decoding with token-level routing,” *arXiv preprint arXiv:2502.01976*, 2025.
- [31] S. Oh, J. Kim, J. Park, S.-W. Ko, T. Q. Quek, and S.-L. Kim, “Uncertainty-aware hybrid inference with on-device small and remote large language models,” *arXiv preprint arXiv:2412.12687*, 2024.
- [32] X. Gao, J. Zhang, L. Mouatadid, and K. Das, “Spuc: Perturbation-based uncertainty quantification for large language models,” *arXiv preprint arXiv:2403.02509*, 2024.
- [33] Y. Huang, J. Song, Z. Wang, H. Chen, and L. Ma, “Look before you leap: An exploratory study of uncertainty measurement for large language models,” *arXiv preprint arXiv:2307.10236*, 2023.
- [34] Y. Gal and Z. Ghahramani, “Dropout as a bayesian approximation: Representing model uncertainty in deep learning,” in *international conference on machine learning*, pp. 1050–1059, PMLR, 2016.
- [35] G. A. Miller, “Wordnet: a lexical database for english,” *Communications of the ACM*, vol. 38, no. 11, pp. 39–41, 1995.
- [36] A. Fan, M. Lewis, and Y. Dauphin, “Hierarchical neural story generation,” *arXiv preprint arXiv:1805.04833*, 2018.
- [37] A. L. Gibbs and F. E. Su, “On choosing and bounding probability metrics,” *International statistical review*, vol. 70, no. 3, pp. 419–435, 2002.
- [38] C. L. Canonne, “A short note on an inequality between kl and tv,” *arXiv preprint arXiv:2202.07198*, 2022.
- [39] X. Niu, B. Bai, N. Guo, W. Zhang, and W. Han, “Rate-distortion-perception trade-off in information theory, generative models, and intelligent communications,” *Entropy*, vol. 27, no. 4, p. 373, 2025.
- [40] V. Nair and G. E. Hinton, “Rectified linear units improve restricted boltzmann machines,” in *Proceedings of the 27th international conference on machine learning (ICML-10)*, pp. 807–814, 2010.
- [41] A. Holtzman, J. Buys, L. Du, M. Forbes, and Y. Choi, “The curious case of neural text degeneration,” *arXiv preprint arXiv:1904.09751*, 2019.
- [42] M. Nguyen, A. Baker, C. Neo, A. Roush, A. Kirsch, and R. Schwartz-Ziv, “Turning up the heat: Min-p sampling for creative and coherent llm outputs,” *arXiv preprint arXiv:2407.01082*, 2024.
- [43] C. Tang, J. Liu, H. Xu, and L. Huang, “Top- $n\sigma$: Not all logits are you need,” *arXiv preprint arXiv:2411.07641*, 2024.
- [44] R. T. et al., “Stanford alpaca: An instruction-following llama model,” 2023.
- [45] S. Alaparthi and M. Mishra, “Bidirectional encoder representations from transformers (bert): A sentiment analysis odyssey,” *arXiv preprint arXiv:2007.01127*, 2020.
- [46] S. Longpre et al., “The flan collection: Designing data and methods for effective instruction tuning,” in *International Conference on Machine Learning*, pp. 22631–22648, PMLR, 2023.

- [47] H. Peng, X. Lv, Y. Bai, Z. Yao, J. Zhang, L. Hou, and J. Li, “Pre-training distillation for large language models: A design space exploration,” *arXiv preprint arXiv:2410.16215*, 2024.
- [48] M. A. Zaidi, A. Kedia, J. Ahn, T. Kwon, K. Lee, H. Lee, J. Lee, *et al.*, “Sparse logit sampling: Accelerating knowledge distillation in llms,” *arXiv preprint arXiv:2503.16870*, 2025.
- [49] P. Pajo, “Comprehensive analysis of google’s agent2agent (a2a) protocol: Technical architecture, enterprise use cases, and long-term implications for ai collaboration,” 2025.
- [50] B. Radosevich and J. Halloran, “Mcp safety audit: Llms with the model context protocol allow major security exploits,” *arXiv preprint arXiv:2504.03767*, 2025.